AMERICAN ACADEMY OF OPHTHALMOLOGY®

Computational Imaging Biomarker Correlation with Intraocular Cytokine Expression in Diabetic Macular Edema

Radiomics Insights from the IMAGINE Study

Sudeshna Sil Kar, PhD,[1,2] Joseph Abraham, MD,[1] Charles C. Wykoff, MD, PhD,[3,4] Duriye Damla Sevgi, MD,[1] Leina Lunasco, BS,[1] David M. Brown, MD,[3,4] Sunil K. Srivastava, MD,[1,5] Anant Madabhushi, PhD,[2,6,] Justis P. Ehlers, MD[1,5,*]*

Purpose: Various pathways and cytokines are implicated in pathogenesis of diabetic macular edema (DME). Computational imaging biomarkers (CIBs) of vessel tortuosity from ultra-widefield fluorescein angiography (UWFA) and texture patterns from OCT images have been associated with anti−vascular endothelial growth factor (VEGF) therapy treatment response in DME. This analysis was a radiogenomic assessment of the association between underlying cytokines, UWFA, and OCT-based DME CIBs.

Design: Biclustering analysis based on UWFA and OCT CIBs to identify a common imaging phenotype across patients with subsequent assessment of underlying cytokine signatures and treatment response attributes.

Participants: The IMAGINE DME study was a post hoc study of cytokine expressions that included 24 eyes with sufficient baseline aqueous humor samples and an in-depth assessment of the imaging studies obtained during the phase I/II DmeAntiVEgf study (DAVE) that measured different cytokine expressions.

Methods: A total of 151 graph or morphologic features quantifying leakage shape, size, density, interobject distance, and architecture of leakage spots and 5 vessel tortuosity features were extracted from the baseline UWFA scans, and 494 texture-based radiomics features were extracted from each of the fluid and retinal tissue compartments of OCT images. Biclustering enables simultaneous clustering of patients and features and was used to aggregate patients in terms of their commonality of phenotypes (based on similar imaging attributes) and to identify commonality in terms of cytokine expression and treatment response to anti-VEGF therapy.

Main Outcome Measures: Identification of eyes with similar imaging phenotypes to evaluate commonalities of patterns and underlying cytokine expression.

Results: Strong correlations between VEGF and 7 UWFA leakage morphologic features (Pearson correlation coefficient [PCC], 0.45−0.51; $P < 0.05$), 1 vascular tortuosity-based UWFA feature (PCC, 0.45; $P = 0.00016$), and 2 OCT-derived intraretinal fluid texture features (PCC, 0.58−0.63; $P < 0.05$) were identified. Strong correlation between intraretinal fluid features and other cytokines (PCC, 0.41−0.59; $P < 0.05$) were also observed.

Conclusions: This study identified groups of eyes with similar imaging phenotypes as defined by UWFA and OCT CIBs that demonstrated similar treatment response patterns and cytokine expression, including a strong association between VEGF with UWFA-derived leakage morphologic and vessel tortuosity features. *Ophthalmology Science 2022;2:100123 © 2022 by the American Academy of Ophthalmology. This is an open access article under the CC BY-NC-ND license (http://creativecommons.org/licenses/by-nc-nd/4.0/).*

Supplemental material available at www.ophthalmologyscience.org

Diabetic macular edema (DME) is one of the main causes of visual impairment and blindness worldwide. It affects approximately 14% of patients with diabetes globally.[1] It is characterized by progressive retinal microvascular changes leading to tissue ischemia, increased permeability, neovascularization, edema, and swelling of the central retina (macula). Although the exact pathophysiologic features of DME remain unknown, several factors, such as increased oxidative stress, inflammation, alteration in the blood−retinal barrier, and ultimate vascular dysfunction contribute to the development of DME.[1,2]

Although the molecular pathogenesis of DME is not fully elucidated, vascular endothelial growth factor (VEGF) is one of the primary mediators for the development of DME.[3] Vascular endothelial growth factor has been identified as the primary vasopermeability factor that disrupts and stimulates the breakdown of the intercellular junction of the

https://doi.org/10.1016/j.xops.2022.100123
ISSN 2666-9145/22

blood–retinal barrier.[4] This, in turn, causes the accumulation of intraretinal fluid (IRF) and subretinal fluid. Vascular endothelial growth factor also plays an important role in increased vessel tortuosity and in vascular leakage. Intravitreal aflibercept injections of VEGF inhibitors are now the first-line treatment for DME management. Despite the efficacy of anti-VEGF therapy in improving visual acuity and decreasing retinal thickening, the degree of response to anti-VEGF therapy varies from patient to patient, with many of these patients experiencing rapid significant visual acuity, whereas others may not benefit despite several injections.[5] Apart from VEGF, several other cytokines and pathways, such as hepatocyte growth factor, interleukin 6, interleukin 8, monocyte chemoattractant protein 1 (MCP-1), urokinase plasminogen activator receptor, and angiopoietin-like 4 (ANGPTL4) have also been implicated in the pathophysiologic characteristics of DME.[6] Increased levels of proinflammatory mediators in aqueous humor have been observed for patients with DME compared with patients without DME.[7]

Imaging technologies with both spectral-domain OCT and ultra-widefield angiography (UWFA) provide a critical foundation for assessment of DME. Currently, the use of these data-rich images is restricted primarily to subjective clinician interpretation and basic quantitative measures. The different fluid and retinal tissue compartments of the OCT images contain valuable information in the form of variation of texture, gradient, and heterogeneity. Historically, these compartments have not been readily available for assessment because of challenges in segmentation, but advances in image analysis platform and machine learning enhancements have enabled more advanced evaluations for both OCT and UWFA.[8–13] Subtle variation in morphologic characteristics and alterations in texture within the fluid and the retinal tissue compartments, as well as structural changes in the retina, are well visualized in OCT scans resulting from the underlying disease manifestation. The heterogeneity within the different retinal compartments is well captured by different texture-based radiomics descriptors. However, UWFA enhances visualization of panretinal vascular abnormalities, such as microaneurysms, leakage, and nonperfusion in DME and diabetic retinopathy (DR).[13] Both UWFA and OCT provide a comprehensive assessment of anatomic and retinal vascular impact of DME.

Previous work by our team identified both UWFA and OCT-based radiomic features that are associated with anti-VEGF treatment response and durability in DME. More specifically, new radiomic computational imaging biomarkers (CIBs) specifically focused on characterizing different morphologic properties of leakage areas and tortuosity of vasculature from UWFA scans that were linked to durability of therapy and treatment response.[14] In addition, multi compartmental OCT analysis identified different texture-based radiomic descriptors extracted from the fluid and the retinal tissue compartments that were associated with anti-VEGF therapy response.[15] However, the correlations between these imaging features and intraocular cytokine levels to date have not been investigated thoroughly. The possible associations between underlying expression of specific cytokines and CIBs associated with anti-VEGF response in the context of in-depth phenotypic characterization of both UWFA and OCT CIBs may enable opportunities for targeted therapeutic selection and predictive modeling of progression risk. In this study, in an attempt to provide a molecular and biological basis for the radiomic features, the identification of radiogenomic correlations between cytokine expression and CIBs was sought. Specifically, morphologic features quantifying the shape, size, density, and interobject distance attributes; architecture of the leakage nodes (i.e., global information on the leakage foci arrangement); vessel tortuosity-based features from the UWFA images[14]; and the texture-based OCT-derived radiomic descriptors extracted from the different fluid and the retinal tissue compartments of the OCT images that were previously shown[15] to be associated with response to anti-VEGF therapy for DME were evaluated.

Biclustering is a unique analysis system that allows simultaneous clustering of rows (patients) and columns (features) of a data matrix. In this preliminary study, biclustering was used on UWFA and OCT features independently to identify eyes that were likely to demonstrate a similar morphologic phenotype and potential response pattern to anti-VEGF therapy in DME. After cluster identification, the correlation between the cytokines and the radiomics-based CIBs that were coclustered with the patient subgroups were investigated to establish their biological and molecular basis.

Methods

Study Description and Cytokine Assessment

The IMAGINE DME Study was a post hoc analysis that evaluated aqueous cytokine expression with an in-depth assessment of the imaging studies obtained throughout the phase I/II DmeAntiVEgf study (DAVE) performed by Brown et al.[16] The IMAGINE study was granted exemption by the Cleveland Clinic institutional review board.[8] The DAVE study obtained institutional review board approval (Sterling institutional review board), and all participants provided informed consent. Adherence to the tenets of the Declaration of Helsinki was required for the study. The main objective of this study was to evaluate the association between the baseline cytokine profile of the patients with DME and their corresponding treatment response to anti-VEGF therapy. The DAVE study was a 3-year prospective randomized trial evaluating ranibizumab alone compared to combination therapy with targeted retinal photocoagulation to nonperfusion areas in treatment-naïve eyes with DME. Twenty-four eyes from 20 patients with sufficient baseline aqueous humor samples, UWFA data, and OCT data from the DAVE study were included in the study. The remaining eyes were excluded because of the unavailability of aqueous humor samples, UWFA of sufficient quality for assessment, or both. Included participants had visually significant DME, were 18 years of age or older, and had severe nonproliferative DR or early proliferative DR. All participants received 4 doses of monthly 0.3-mg ranibizumab injections before monthly visits, with re-treatment as required based on disease activity (pro re nata treatment) during the entire course of the study. Baseline aqueous fluid samples were obtained at the time of initial intravitreal therapy as part of the DAVE study. Samples were stored at −80 °C until analysis. For this analysis, 2 multiplex arrays measured levels in quadruplicate for cytokine quantification (RayBiotech). Because urokinase

plasminogen activator receptor, VEGF, ANGPTL4, hepatocyte growth factor, interleukin 6, MCP-1, tissue inhibitor of metalloproteinase (TIMP)-1, and TIMP-2 are key cytokines implicated in the pathogenesis of DME, these 8 cytokines were selected for correlation analysis. Subsequently, the correlation between these 8 cytokines and the radiomics-based CIBs that were coclustered with the patient subgroups in each of the biclusters was investigated to establish the biological and molecular basis of the biclusters and CIBs.

Quantitative Ultra-Widefield Fluorescein Angiography Analysis and Higher-Order OCT Analysis

For UWFA analysis, image analysis experts selected optimal mid-frame and late-frame UWFA images. Selection was performed based on centration, field of view, timing of angiographic study, and image clarity. After image selection, a machine learning-enhanced leakage segmentation platform was used to identify leakage foci and to segment each leakage node (i.e., object), as previously described.[9,11,13,17]

The baseline macular OCT cube was evaluated using a machine learning-enhanced, automated, multilayer feature extraction segmentation platform with expert review and segmentation correction as needed. Retinal anatomic layers, including ellipsoid zone integrity and fluid objects, were extracted, as previously described.[8,13]

Categorization of Eyes Based on Treatment Response

Based on therapeutic response, eyes were categorized into 4 different groups: super responders, early responders, slow responders, and nonresponders, as previously described.[8] For super responders and early responders, the IRF volume was reduced by $> 80\%$ or to < 0.001 mm^3, the excess thickening of the central subfield thickness was reduced by 80% after month 1 (for super responders) or by month 3 (for early responders), or both. Based on this criteria, the super and early responders were combined as optimal responders. The slow responders and nonresponders were combined as minimal responders. Thirteen patients were optimal responders and 11 patients were minimal responders. Baseline VEGF levels were significantly higher among the optimal responders compared with the minimal responders (848.2 pg/ml vs. 374.5 pg/ml; $P = 0.018$). Therefore, in the present study, we considered the optimal responders and the minimal responders to belong to the high VEGF group (n = 13) and low VEGF group (n = 11), respectively, to assess their common morphologic and response patterns to anti-VEGF therapy.

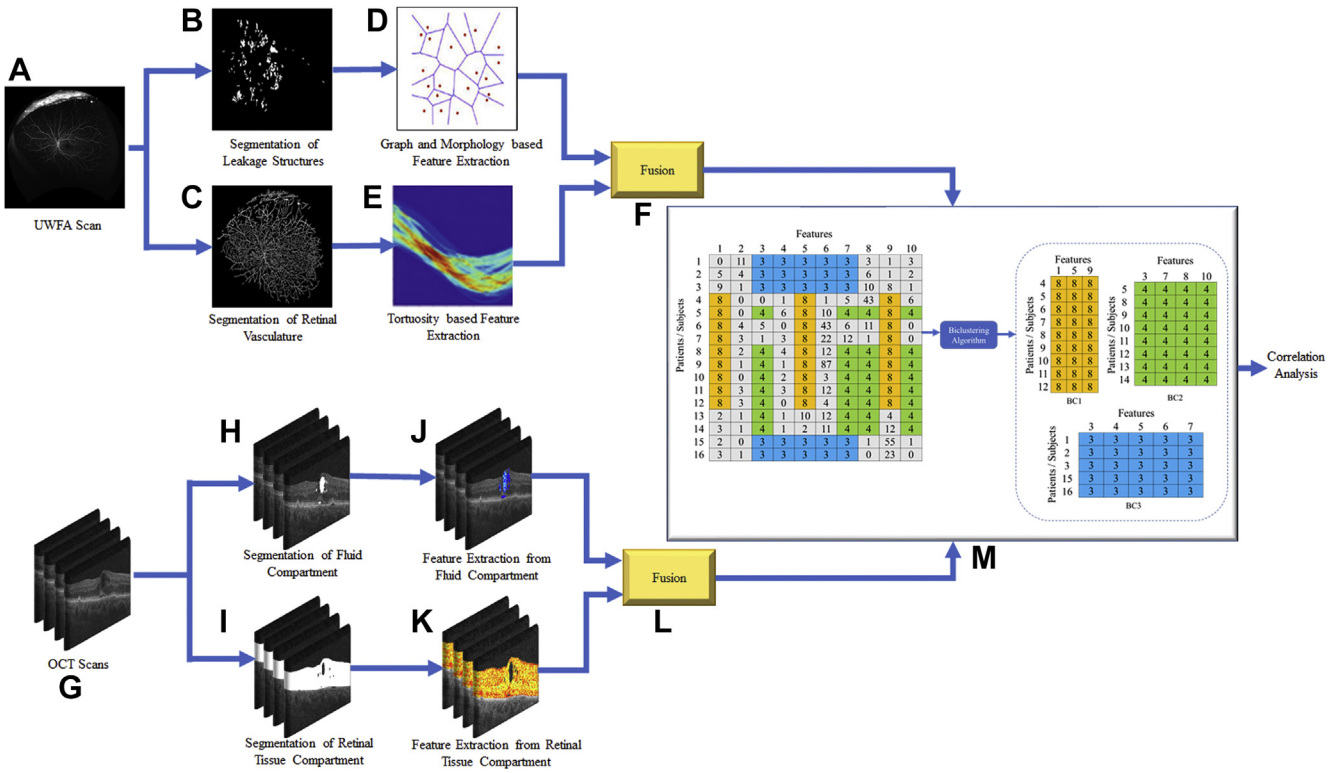

Figure 1. Diagram showing workflow of the ultra-widefield fluorescein angiography (UWFA)-derived leakage and vessel tortuosity features and OCT-derived spatial radiomic features from the IMAGINE Diabetic Macular Edema Study and corresponding evaluation: (**A**) original UWFA scan, (**B**) segmentation of leakage structure, (**C**) segmentation of retinal vasculature, (**D**) graph and morphologic feature-based feature extraction from leakage structures, (**E**) vessel tortuosity-based feature extraction, (**F**) fusion of leakage and tortuosity features, (**G**) original OCT scans, (**H**) segmentation of fluid, and (**I**) segmentation of retinal tissue compartments, (**J**) feature extraction from fluid, and (**K**) feature extraction from retinal tissue compartments, (**L**) fusion of fluid and retinal tissue features, and (**M**) biclustering of OCT and UWFA features. Each bicluster identifies a patient group with similar diagnostic patterns. The correlation between the features identified by biclusters and different cytokine levels was evaluated.

Table 1. Summary of Association between Ultra-Widefield Fluorescein Angiography Features and Cytokines

Bicluster No.	Ultra-Widefield Fluorescein Angiography Features	Cytokines	Pearson Correlation Coefficient	P Value
1	Leakage shape: mean invariant moment 1	VEGF	0.46	0.034
	Leakage shape: mean invariant moment 2		0.45	0.043
	Leakage shape: median invariant moment 4		0.51	0.00012
	Leakage graph: median standard deviation of distance		0.45	0.043
	Leakage shape: standard deviation Fourier descriptor 2		0.48	0.03
	Leakage shape: mean area ratio	MCP-1	−0.46	0.03
2	Leakage shape: mean invariant moment 2	VEGF	0.45	0.043
	Leakage shape: median standard deviation of distance		0.45	0.043
	Vessel tortuosity: variance of inclination, θ		0.45	0.00016

MCP-1 = monocyte chemoattractant protein 1; VEGF = vascular endothelial growth factor.

Overview of the Computational Imaging Feature Extraction Workflow

The computational workflow of the present work is illustrated in Figure 1. For UWFA images, the preprocessing and segmentation of the leakage regions and the vasculature network were completed (Fig 1B, C) on the baseline images (Fig 1A). For the OCT scans (Fig 1G), the fluid and the retinal tissue compartments were segmented (Fig 1H, I). The detailed description of the image analysis and leakage area, vessel, fluid, and retinal tissue compartment segmentation is presented in the Supplemental Appendix (section I). Unique leakage morphologic features and vessel tortuosity-based features were extracted from the baseline UWFA images (Fig 1D, E). For the OCT images, texture-based radiomics features were extracted from each of the fluid compartments (subretinal fluid and IRF) and various retinal tissue compartments (i.e., inner limiting membrane to ellipsoid zone, ellipsoid zone to retinal pigment epithelium, and inner limiting membrane to retinal pigment epithelium; Fig 1J, K) of the OCT scans. The UWFA and OCT features (Fig 1F, L) were biclustered independently (Fig 1M) and their association with the cytokines was investigated for radiogenomic analysis.

Radiomics Feature Extraction

Ultra-Widefield Fluorescein Angiography Image Features. For quantitative measurement of leakage shapes and their spatial distribution, proximity metrics using graph network analysis were computed and morphologic features quantifying shape, size, and density attributes of the leakage areas were extracted as previously described.[14] The graph features (F_g) were derived from the leakage centroid coordinates. This family included 51 descriptors of leakage arrangement and density-derived measurements as quantitative features to describe the leakage spots. The morphologic features (F_m) included 25 measurements of objects or area distance to N nearest neighbors, disorder of distance to N neighbors, invariant and Fourier descriptors of boundary points, fractal dimension, smoothness, area, and perimeter. The mean, median, standard deviation, and minimum and maximum ratio of these 25 measurements were calculated. In addition, 5 vascular tortuosity-based features (F_t) were extracted from the baseline UWFA images. Local measures of vessel curvature in the Hough parameter space were computed to model the architectural disorder of the vascular network.[23] The graph features (F_g), morphologic features (F_m), and tortuosity features (F_t) were fused to obtain the entire UWFA feature set (F_{UWFA}).

OCT Image Features. For quantitative feature extraction from the OCT images, a total of 494 3-dimensional texture-based radiomics features were extracted from each of the fluid subcompartment (I_F) and retinal subcompartment (I_{RTC}) subvolumes on a Matlab version 2015b platform (Mathworks, Natick, MA) and fused together to obtain the entire OCT feature set (F_{OCT}). The OCT feature set (F_{OCT}) for every study included 65 Haralick features (capturing texture heterogeneity), 152 Laws energy features (capturing presence of spots, edges, waves, and ripples), 225 Gabor wavelet features (capturing structural detail at different orientations and scales), and 52 Collage features (capturing anisotropic tensor gradient differences). Statistics of median, standard deviation, skewness, and kurtosis were then calculated from the feature within all regions of interest. To remove redundant or collinear features, all possible combinations of features were tested for correlation by calculating the Pearson correlation coefficient (PCC) and those features corresponding to feature pairs with a PCC of > 0.8 were eliminated. All feature values were normalized (mean of 0 and standard deviation of 1). Detailed descriptions of the UWFA-derived graph, morphology-based leakage, vessel tortuosity, and the texture-based OCT features are provided in the Supplemental Appendix (sections II, III, IV, and V, respectively).

Morphologic Phenotype Biclustering

Biclustering enables simultaneous clustering of patients and features.[18,19] Each bicluster is represented as a homogeneous submatrix of the imaging features (Supplemental Appendix, section VI). In this study, biclustering of patients and the UWFA feature set (F_{UWFA}) and OCT feature set (F_{OCT}) was performed simultaneously to identify the subsets that had similar imaging phenotypes and response attributes or cytokine expression. The biclusters discovered from the radiomic features represent a common imaging phenotype across patients within the subgroup. For biclustering, the BiclustGUI R package version 1.1.3 was used, a graphical user interface developed as a plug-in for R Commander. We implemented the different biclustering methods such as Plaid, CC, XMotif, Spectral, QuestMotif, and BiMax within the biclust package.

Three biclusters (bicluster 1 and bicluster 2 from UWFA features (F_{UWFA}) and bicluster 3 from OCT features (F_{OCT})) from the consensus of these 6 bicluster methods were identified. In bicluster 1 and bicluster 2, a subset of patients with similar expression patterns of F_{UWFA} were coclustered. Similarly, bicluster 3 involved coclustering of a subset of patients with similar expression patterns of F_{OCT}. The PCC values and the associated P values between F_{UWFA} and F_{OCT} (that were coclustered in each bicluster) and the measured cytokines were calculated to determine whether the features identified by biclustering were biologically and clinically relevant. The Benjamini-Hochberg method was used to adjust the P values and control for the false discovery rate.[20] Statistically significant associations with $P < 0.05$ and absolute value of PCC > 0.4 were reported.

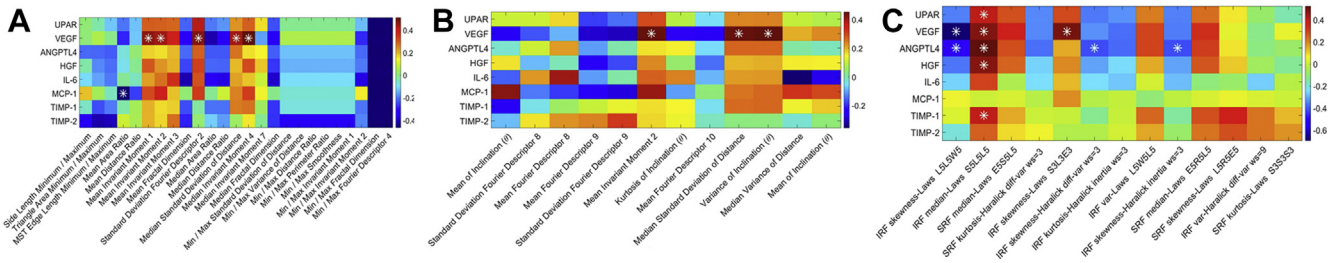

Figure 2. Pearson correlation coefficient matrix showing the association between the cytokine levels and the ultra-widefield fluorescein angiography (UWFA) features identified by (**A**) bicluster 1 and (**B**) bicluster 2, respectively, and (**C**) the texture-based OCT features identified by bicluster 3. Strong association between vascular endothelial growth factor (VEGF) and leakage shape and vessel tortuosity-based UWFA features and between VEGF and texture-based OCT features are observed. *Statistically significant ($P < 0.05$) relationship. ANGPTL4 = angiopoietin-like 4; HGF = hepatocyte growth factor; IL = interleukin; IRF = intraretinal fluid; Max = maximum; MCP-1 = monocyte chemoattractant protein 1; Min = minimum; MST = minimum spanning tree; SRF = subretinal fluid; TIMP = tissue inhibitor of metalloproteinase; UPAR = urokinase plasminogen activator receptor.

Results

Association of Ultra-Widefield Fluorescein Angiography-Based Radiomic Descriptors with Cytokine Levels

From the consensus of the biclustering methods, 2 UWFA-based biclusters (bicluster 1 and bicluster 2) were identified. In bicluster 1, 10 eyes (8 from the high VEGF group and 2 from the low VEGF group) and 25 UWFA morphology-based features (F_m) were coclustered. Among these, 6 features were identified to have significant association ($P < 0.05$) with VEGF and MCP-1 with PCC of > 0.4 or PCC of < -0.4. In bicluster 2, all the eyes from the high VEGF group and 12 UWFA CIBs (F_{UWFA}) were coclustered. Three of these UWFA features (2 morphologic and 1 tortuosity) were found to be associated with VEGF ($P < 0.05$, PCC > 0.4). The details of these associations are presented in Table 1.

The relationship matrix between the cytokine levels and the radiomics features (F_{UWFA} and F_{OCT}) are illustrated in Figure 2. Among the features co-clustered in bicluster 1, the strongest association was found between VEGF and a leakage shape feature (i.e., median invariant moment 4 [PCC, 0.51; $P = 0.00012$]; Fig 3A). This specific shape-feature CIB captures the leakage node appearance and boundary characteristics. The shape of the leakage objects for the high VEGF group tend to be more radial (possibly perivascular in origin) as compared with the low VEGF group (Fig 4A).

Among the features coclustered in bicluster 2, the strongest association was identified between VEGF and a tortuosity metric (i.e., variance of inclination θ [PCC, 0.45; $P = 0.00016$]; Fig 3). Higher variance in this UWFA CIB represents greater disorder and more twisted vessel architecture and vice versa. More complex and twisted tortuosity patterns were observed for the high VEGF group, as shown in Fig 4.

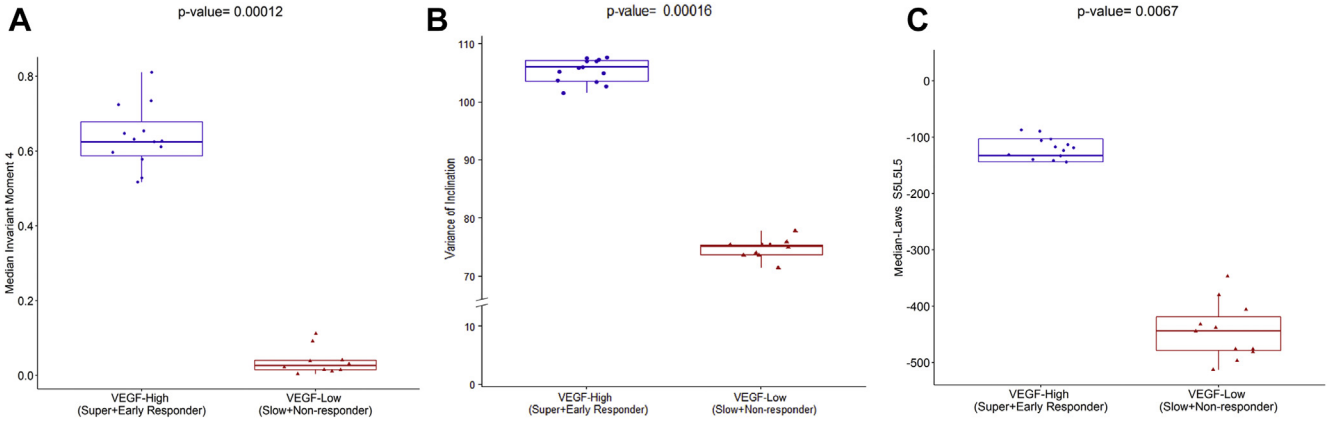

Figure 3. Ultra-widefield fluorescein angiography (UWFA) feature assessment with cytokine expression. **A**, Leakage feature assessment on baseline UWFA image for 1 eye in the high vascular endothelial growth factor (VEGF) group (super plus early responder) and low VEGF group (slow plus nonresponder). The centroid of the leakage patch is highlighted in red and the boundary of each of the leakage patches are highlighted in separate colors. Leakage patches with same area are presented using the same color. **B**, Vessel tortuosity assessment on baseline UWFA image for 1 eye in the high VEGF group and low VEGF group. As observed, vessels in the high VEGF group are more tortuous compared with the vessels in the low VEGF group. **C**, Feature map showing texture-based OCT-derived laws S5L5L5 feature for 1 eye from the high VEGF group and low VEGF group. Higher feature expression is observed for the high VEGF group.

Association of OCT-Based Radiomic Descriptors with Cytokine Levels

From the consensus biclustering methods, bicluster 3 was identified based on OCT radiomics features (F_{OCT}) and involved coclustering of 8 eyes (6 from the high VEGF group and 2 from the low VEGF group) and 13 texture-based OCT features. Ten of these textural features were found to have significant association ($P < 0.05$) with different cytokines with PCC of > 0.4 <-0.4. These associations were all between (1) VEGF and IRF texture-based radiomics features (i.e., skewness laws L5L5W5 [PCC, −0.67; $P = 0.0002$], median laws S5L5L5 [PCC, 0.63; $P = 0.0067$], and skewness laws S3L3E3 [PCC, 0.58; $P = 0.02$]). In addition to VEGF, associations were identified between (1) urokinase plasminogen activator receptor and IRF texture-based features (median laws S5L5L5 [PCC, 0.59; $P = 0.04$]), (2) ANGPTL4 and 4 IRF texture-based features (skewness laws L5L5W5 [PCC, −0.49; $P = 0.02$], median laws S5L5L5 [PCC, 0.53; $P = 0.008$], skewness Haralick difference variance [PCC, −0.42; $P = 0.04$], and skewness Haralick inertia [PCC, −0.42; $P = 0.04$]), (3) hepatocyte growth factor and IRF texture-based features (median laws S5L5L5 [PCC, 0.47; $P = 0.02$]), and (4) TIMP-1 and IRF-based texture features (median laws S5L5L5 [PCC, 0.41; $P = 0.004$]).

The relationship matrix between cytokine levels and the OCT features identified by bicluster 3 is illustrated in Figure 2C. The strongest correlation was identified between VEGF and an IRF texture feature (i.e., IRF medians laws S5L5L5 [PCC, 0.63; $P = 0.0067$]; Fig 3C). This texture feature represents the Laws energy-based textural patterns of spots in the horizontal direction and levels in the vertical and diagonal direction using a convolution filter. As observed from Fig 4C, this texture-based feature descriptor is highly expressed for the high VEGF group. Scatterplots depicting the association between VEGF and UWFA- and OCT-based CIBs are presented in Figure 5. Scatterplots showing the association between other cytokines and UWFA- and OCT-based CIBs are presented in the Supplemental Fig 1.

Discussion

This study investigated the link between aqueous humor cytokine levels and therapeutic response to anti-VEGF therapy for eyes with DME, as well as the biological

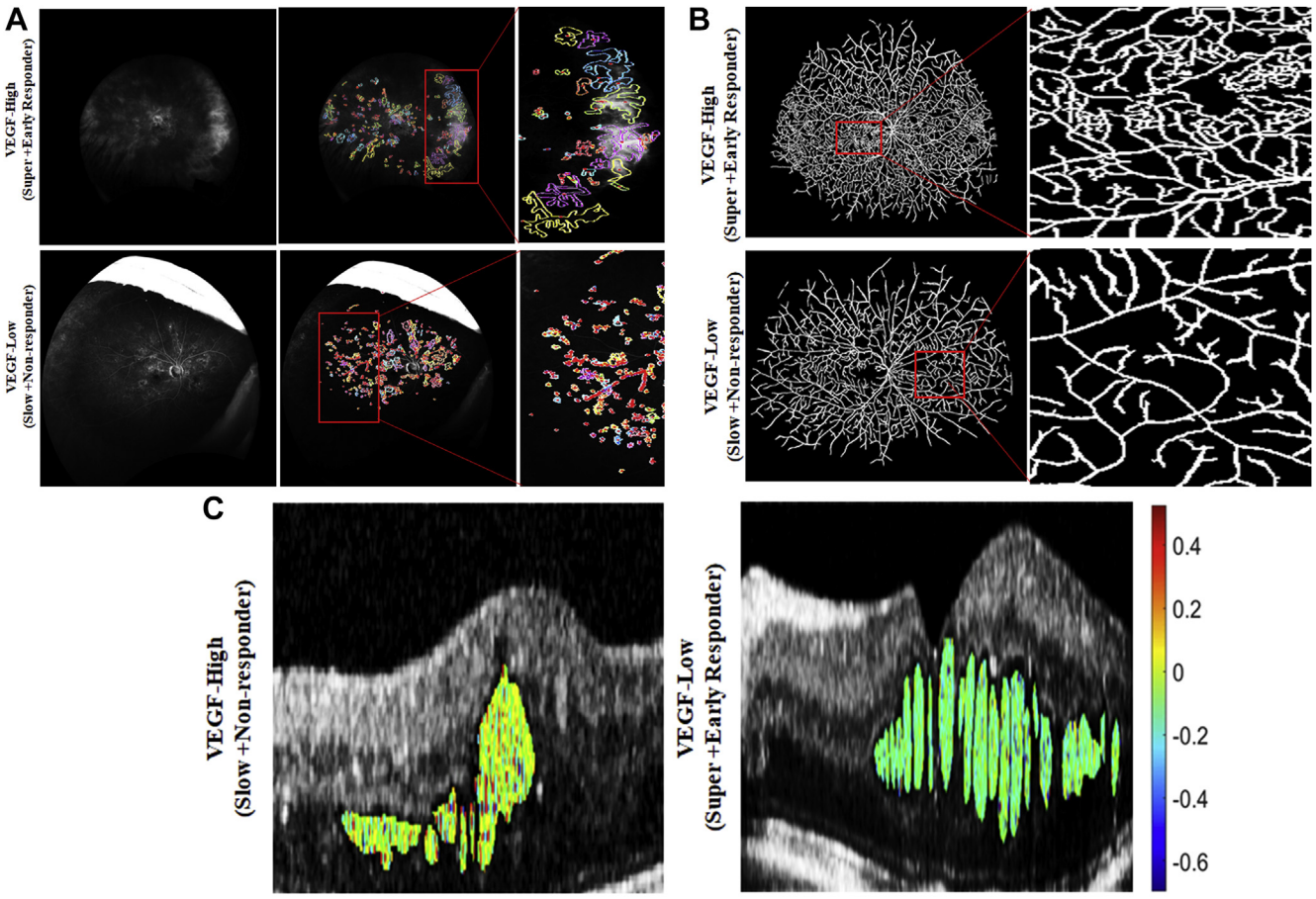

Figure 4. Box-and-whisker plots showing the (**A**) leakage shape feature median invariant moment 4, (**B**) vessel tortuosity feature variance of inclination, and (**C**) the texture-based OCT feature median laws S5L5L5, which were found to be strongly correlated with vascular endothelial growth factor (VEGF). The plot on the left and right corresponds to the feature values from the high VEGF group (n = 13) and low VEGF group (n = 11), respectively.

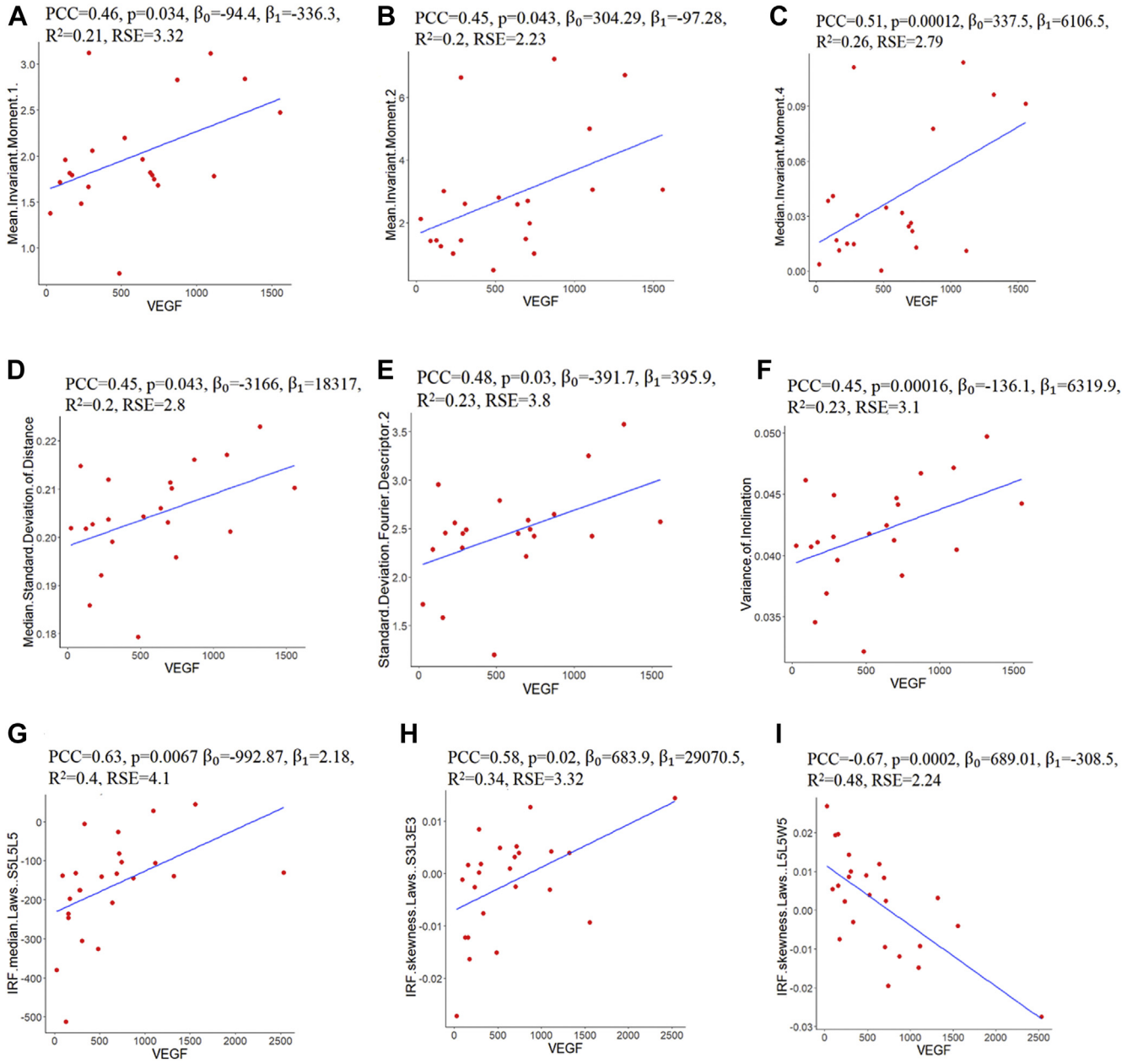

Figure 5. Scatterplot visualizations showing the correlation between vascular endothelial growth factor (VEGF) and (**A**–**E**) ultra-widefield fluorescein angiography (UWFA)-derived leakage shape-based computational imaging biomarkers (CIBs), (**F**) UWFA-derived vessel tortuosity-based CIB, and (**G**–**I**) OCT-derived texture-based CIBs. β_0, β_1 = regression or β coefficients; IRF = intraretinal fluid; PCC = Pearson correlation coefficient; RSE = residual standard error.

underpinning of different UWFA- and OCT-derived CIBs through correlation with the cytokine levels. Although cytokines provide a direct measure of biologic activity, our understanding of the link to clinical phenotype and progression of DME remains incomplete. Despite extensive research on aqueous humor cytokines, substantial variations exist in the results reported on the predictive response of anti-VEGF therapy for patients with DME.[5,21,22] In addition, findings reported on whether increased or decreased aqueous humor VEGF level is associated with the treatment response of anti-VEGF therapy are contradictory. Several of the studies identified baseline differences between eyes that are responders and nonresponders to anti-VEGF therapy, whereas others did not.[5,21] In a recent study,[8] OCT-based imaging biomarkers were correlated with both intraocular cytokines and responsiveness to anti-VEGF therapy, which suggested a possible link between imaging phenotypes and underlying biological pathways as well as their potential link to DME prognosis. Baseline concentrations of VEGF and MCP-1 were also found to be associated with anatomic response to anti-VEGF therapy. Two additional studies[21,24] found higher concentrations of VEGF in responders to

anti-VEGF therapy compared with nonresponders. In a seemingly contradictory finding, a separate study identified a statistically significant relationship between lower aqueous humor VEGF concentration and long-term anatomic response of eyes with DME treated with anti-VEGF therapy.[25] Kwon and Jee[22] also did not identify baseline VEGF as a predictive factor of anti-VEGF therapy. Given the inconsistency, further investigation is needed to explore the potential role of cytokines, including VEGF, in the pathogenesis of DME that may clarify the discrepancies reported in the literature. Further, current technologies require invasive sampling and testing to identify a specific cytokine; opportunities for noninvasive exploration of cytokine expression, such as a surrogate imaging biomarker, could have significant value.

Radiomics, the high-throughput automated extraction of subvisual features from images, recently showed promising results in disease prognosis and treatment response assessment in various clinical domains as reported by our group and others.[26–28] Numerous previous studies demonstrated the effect of anti-VEGF therapy on retinal vasculature and leakage patterns as well.[29,30] These studies explored several structural and morphologic characteristics of UWFA images or OCT leakage in an attempt to understand the effect of anti-VEGF on retinal fluid accumulation. In a recent study,[14] quantitative vessel tortuosity metrics on UWFA images from treatment-naïve eyes demonstrated the feasibility of identifying rebounders (nonresponders) from nonrebounders (responders) with dosing extension in the PERMEATE clinical study.[9,31] In addition, spatial arrangement of leakage areas on UWFA was found to distinguish the nonresponders from the responders.[14] In a related study, features quantifying proximity of each leakage foci to main retinal vessels and the optical nerve were predictive of response to anti-VEGF therapy.[32] Establishing the molecular underpinning of CIBs by identification of pathways significantly associated with the imaging biomarkers may help in predicting patient outcomes, alleviating treatment burden, and increasing cost effectiveness and more personalized treatment. Consequently, in this preliminary study, assessment of the aggregation of patients with similar morphologic and response attributes, as well as the radiogenomic correlations between the leakage morphologic and vessel tortuosity-based UWFA features and texture-based compartmental radiomic descriptors of the OCT images with the cytokine pathways, was carried out to establish their molecular and biological basis.

Patients with similar morphologic phenotypes and response attributes were identified using biclustering. Three biclusters were identified: 2 biclusters from the UWFA features and 1 bicluster from the OCT features. Most of the patients in the high VEGF group were found to be coclustered in these 3 biclusters, which suggests that the eyes in the high VEGF group have similar subvisual imaging phenotypes. In this report, the radiomic features that correlated strongly with VEGF were descriptors of leakage shape, vessel tortuosity, and IRF texture. This suggests that there may be unique differences in the spatial arrangement of leakage patterns between the eyes that are more likely to respond to anti-VEGF therapy than those that do not. This finding also corroborates previous related findings[14] in which leakage characteristics were found to be associated with treatment response to anti-VEGF therapy. Higher disorder and more complex and twisted tortuosity patterns of retinal blood vessels were observed for the eyes with high VEGF, a known visual feature associated with VEGF levels. This supports the notion that subtle variations may exist in the local vessel orientations that may be implicated with anti-VEGF treatment response and durability. This finding also corroborates our previous finding[14], in which inherent difference in the local vessel tortuosity was observed among the patients treated with anti-VEGF therapy.

Texture-based radiomics features pertaining to the IRF subcompartment were highly correlated with VEGF level. Higher expression of texture-based features (i.e., Laws energy descriptors) were found in the high VEGF group, suggesting the presence of complex and convoluted architecture in the texture of the IRF subcompartment with high VEGF, whereas more homogeneity in the tissue morphologic features is preserved for eyes with low VEGF. The strong correlation between different cytokines and the UWFA feature set and OCT feature set suggests that the effect of the cytokines in the pathogenesis of DME and DR can be assessed by analyzing multiple UWFA- and OCT-based CIBs.[14,15]

Although these preliminary results are promising, the current study has a number of limitations that should be discussed. An important limitation to recognize is the small sample size (n = 24). Additionally, given the complexity of the biclustering-based assessment and the small number of fellow eyes (n = 4), intereye correlation was not able to be considered, and a larger prospective dataset is needed to validate these findings. That said, the scarcity and high-value aspects of combined aqueous cytokine and high-quality imaging are critical components of the value of this analysis. Another limitation is that the impact of subtle changes in segmentation is not clear, although our initial studies seem to suggest that the features were resilient to slight changes in the segmentation results. Nonetheless, this is the novel study to look at this radiogenomic association in the context of DME. Beyond demonstrating feasibility, some extremely interesting associations were identified, especially as they relate to the association of vascular tortuosity-related features with VEGF levels and the likelihood of response.

This preliminary report provided exciting evidence for the presence of a strong link between VEGF levels and retinal leakage morphologic features, vessel tortuosity, and heterogeneity within the IRF compartments of the OCT scans. This study further established the anatomic–biologic bridge between underlying molecules and higher-order radiomic features. With further validation, these radiomic-based imaging biomarkers could potentially be used for timely personalized disease characterization and treatment management of DME.

Acknowledgement

The authors would like to thank Nathaniel Braman and Prateek Prasanna for their contribution in developing the model to compute the architectural disorder of vessel network.

Footnotes and Disclosures

Originally received: April 24, 2021.
Final revision: January 22, 2022.
Accepted: January 27, 2022.
Available online: February 4, 2022. Manuscript no. XOPS-D-21-00076.

[1] The Tony and Leona Campane Center for Excellence in Image-Guided Surgery and Advanced Imaging Research, Cole Eye Institute, Cleveland Clinic, Cleveland, Ohio.

[2] Department of Biomedical Engineering, Case Western Reserve University, Cleveland, Ohio.

[3] Retina Consultants of Texas, Retina Consultants of America, Houston, Texas.

[4] Blanton Eye Institute, Houston Methodist Hospital, Houston, Texas.

[5] Vitreoretinal Service, Cole Eye Institute, Cleveland Clinic, Cleveland, Ohio.

[6] Louis Stokes Cleveland Veterans Administration Medical Center, Cleveland, Ohio.

*Both authors contributed equally as senior authors.

Disclosure(s):

All authors have completed and submitted the ICMJE disclosures form.

The author(s) have made the following disclosure(s): C.C.W.: Consultant – Alimera Sciences, Allegro, Allergan, Alynylam, Apellis, Bayer, Clearside, D.O.R.C., EyePoint, Genentech/Roche, Kodiak, Notal Vision, Novartis, ONL Therapeutics, PolyPhotonix, RecensMedical, Regeneron, Regenxbio, Santen; Financial support – Adverum, Allergan, Apellis, Clearside, EyePoint, Genentech/Roch, Neurotech, Novartis, Opthea, Regeneron, Regenxbio, Samsung, Santen; Lecturer – Regeneron

D.M.B.: Consultant – Regeneron, Bayer, Senju, Allergan, Optos, Zeiss, Heidelberg, OHR, Biotime, Gemini, Genentech/Roche, Novartis, Apellis, Regenxbio, Chengdu Kanghong Biotechnology; Financial support – Adverum, Allergan, Apellis, Clearside, Genentech/Roch, Novartis, Opthea, Regeneron, Regenxbio, Samsung, Santen

S.K.S.: Consultant – Bausch & Lomb, Novartis, Regeneron; Financial support – Regeneron, Allergan, Gilead

A.M.: Consultant – Aiforia; Financial support – Astrazeneca, Bristol Myers-Squibb, Philips; Equtiy owner – Inspirata, Inc., Elucid Bioimaging

J.P.E.: Consultant – Aerpio, Adverum, Alcon, Allegro, Allergan, Genentech/Roche, Stealth, Novartis, Thrombogenics/Oxurion, Leica, Zeiss, Regeneron, Santen; Financial support – Aerpio, Alcon, Thrombogenics/Oxurion, Regeneron, Genentech, Novartis, Allergan; Patent – Leica

Supported by the National Institutes of Health, Bethesda, Maryland (grant nos.: K23-EY022947, 1U24CA199374-01, R01CA202752-01A1, R01CA208236-01A1, R01CA216579-01A1, R01 CA220581-01A1, and 1U01 CA239055-01; Regeneron, Inc., Tarrytown, New York (grant no.: REGE1901); Research to Prevent Blindness, Inc., New York, New York (unrestricted grant no.: RPB1508DM [Cole Eye Institute]); and the Betty J. Powers Retina Research Fellowship. All study decisions were made independently of funding sources.

HUMAN SUBJECTS: Human subjects were included in this study. The IMAGINE study was granted institutional review board exemption by the Cleveland Clinic institutional review board. The DAVE Study obtained institutional review board approval (Sterling institutional review board) and all subjects provided informed consent. All research adhered to the tenets of the Declaration of Helsinki.

No animal subjects were included in this study.

Author Contributions:

Conception and design: Kar, Wykoff, Srivastava, Madabhushi, Ehlers

Analysis and interpretation: Kar, Abraham, Wykoff, Sevgi, Lunasco, Brown, Srivastava, Madabhushi, Ehlers

Data collection: Kar, Abraham, Wykoff, Sevgi, Lunasco, Brown, Srivastava, Madabhushi, Ehlers

Obtained funding: Ehlers

Overall responsibility: Kar, Abraham, Wykoff, Sevgi, Lunasco, Brown, Srivastava, Madabhushi, Ehlers

Abbreviations and Acronyms:
ANGPTL4 = angiopoietin-like 4; **CIB** = computational imaging biomarker; **DME** = diabetic macular edema; **DAVE** = DmeAntiVEgf study; **DR** = diabetic retinopathy; **IRF** = intraretinal fluid; **MCP-1** = monocyte chemoattractant protein 1; **PCC** = Pearson correlation coefficient; **UWFA** = ultra-widefield fluorescein angiography; **VEGF** = vascular endothelial growth factor.

Keywords:
Diabetic macular edema, OCT, Radiomics, Ultra-widefield fluorescein angiography, Cytokine.

Correspondence:
Justis P. Ehlers, Cole Eye Institute, Cleveland Clinic, 9500 Euclid Avenue/Desk i32, Cleveland, OH 44195. E-mail: ehlersj@ccf.org.

References

1. Klein R, Klein B, Moss S, Cruickshanks K. The Wisconsin epidemiologic study of diabetic retinopathy XV: the long-term incidence of macular edema. *Ophthalmology*. 1995;102(1):7–16.
2. Romero-Aroca P, Baget-Bernaldiz M, Pareja-Rios A, et al. Diabetic macular edema pathophysiology: vasogenic versus inflammatory. *J Diabetes Res*. 2016;2016:2156273. https://doi.org/10.1155/2016/2156273. Epub 2016 Sep 28.
3. Wong TY, Cheung CM, Larsen M, et al. Diabetic retinopathy. *Nat Rev Dis Primers*. 2016;2:16012.
4. Nguyen QD, Brown DM, Marcus DM, et al. Ranibizumab for diabetic macular edema: results from 2 phase III randomized trials: rise and ride. *Ophthalmology*. 2012;119(4):789–801.
5. Hillier RJ, Ojaimi E, Wong DT, et al. Aqueous humor cytokine levels and anatomic response to intravitreal ranibizumab in diabetic macular edema. *JAMA Ophthalmol*. 2018;136(4):382–388.
6. Wu J, Zhong Y, Yue S, et al. Aqueous humor mediator and cytokine aberrations in diabetic retinopathy and diabetic macular edema: a systematic review and meta-analysis. *Dis Markers*. 2019;2019:6928524.
7. Dong N, Xu B, Chu L, Tang X. Study of 27 aqueous humor cytokines in type 2 diabetic patients with or without macular edema. *PLoS One*. 2015;10(4):e0125329.
8. Abraham JE, Wykoff CC, Arepalli S, et al. Aqueous cytokine expression and higher order OCT biomarkers: assessment of the anatomic-biologic bridge in the IMAGINE DME Study. *Am J Ophthalmol*. 2021;222:328–339.
9. Figueiredo N, Srivastava SK, Singh RP, et al. Longitudinal panretinal leakage and ischemic indices in retinal vascular

disease after aflibercept therapy: the PERMEATE Study. *Ophthalmol Retina*. 2020;4(2):154−163.
10. Babiuch A, Wykoff CC, Hach J, et al. Longitudinal panretinal microaneurysm dynamics on ultra-widefield fluorescein angiography in eyes treated with intravitreal aflibercept for proliferative diabetic retinopathy in the recovery study. *Br J Ophthalmol*. 2021;105(8):1111−1115.
11. Babiuch AS, Wykoff CC, Srivastava SK, et al. Retinal leakage index dynamics on ultra-widefield fluorescein angiography in eyes treated with intravitreal aflibercept for proliferative diabetic retinopathy in the recovery study. *Retina*. 2020;40(11):2175−2183.
12. Ehlers JP, Uchida A, Hu M, et al. Higher-order assessment of OCT in diabetic macular edema from the VISTA Study: ellipsoid zone dynamics and the retinal fluid index. *Ophthalmol Retina*. 2019;3(12):1056−1066.
13. Ehlers JP, Jiang AC, Boss JD, et al. Quantitative ultra-widefield angiography and diabetic retinopathy severity: an assessment of panretinal leakage index, ischemic index and microaneurysm count. *Ophthalmology*. 2019;126(11):1527−1532.
14. Prasanna P, Bobba V, Figueiredo N, et al. Radiomics-based assessment of ultra-widefield leakage patterns and vessel network architecture in the PERMEATE study: insights into treatment durability. *Br J Ophthalmol*. 2021;105(8):1155−1160.
15. Kar SS, Sevgi DD, Dong V, et al. Multi-compartment spatially-derived radiomics from optical coherence tomography predict anti-VEGF treatment durability in macular edema secondary to retinal vascular disease: preliminary findings. *IEEE J Transl Eng Health Med*. 2021;9:1000113: PMID: 34350068; PMCID: PMC8328398. https://doi.org/10.1109/JTEHM.2021.3096378.
16. Brown DM, Ou WC, Wong TP, et al. Targeted retinal photocoagulation for diabetic macular edema with peripheral retinal nonperfusion: three-year randomized DAVE Trial. *Ophthalmology*. 2018;125(5):683−690.
17. Ehlers JP, Wang K, Vasanji A, et al. Automated quantitative characterisation of retinal vascular leakage and microaneurysms in ultra-widefield fluorescein angiography. *Br J Ophthalmol*. 2017;101(6):696−699.
18. Huang Q, Huang X, Kong Z, et al. Bi-phase evolutionary searching for biclusters in gene expression data. *IEEE Trans Evol Comput*. 2019;23(5):803−814.
19. Pontes B, Giráldez R, Aguilar-Ruiz J-S. Biclustering on expression data: a review. *J Biomed Inform*. 2015;57:163−180.
20. Benjamini Y, Hochberg Y. Controlling the false discovery rate: a practical and powerful approach to multiple testing. *J R Stat Soc Series B Stat Methodol*. 1995;57:289−300.
21. Shimura M, Yasuda K, Motohashi R, et al. Aqueous cytokine and growth factor levels indicate response to ranibizumab for diabetic macular oedema. *Br J Ophthalmol*. 2017;101(11):1518−1523.
22. Kwon JW, Jee D. Aqueous humor cytokine levels in patients with diabetic macular edema refractory to anti-VEGF treatment. *PLoS One*. 2018;13(9):e0203408.
23. Braman N, Prasanna P, et al. Vascular Network Organization via Hough Transform (VaNgOGH): A Novel Radiomic Biomarker for Diagnosis and Treatment Response. *Medical Image Computing and Computer Assisted Intervention − MICCAI 2018.Lecture Notes in Computer Science. Springer International Publishing; 2018*. 2018:803−811. https://doi.org/10.1007/978-3-030-00934-2_89.
24. Udaondo P, Hernández C, Briansó-Llort L, et al. Usefulness of liquid biopsy biomarkers from aqueous humor in predicting anti-VEGF response in diabetic macular edema: results of a pilot study. *J Clin Med*. 2019;8(11):1841.
25. Felfeli T, Juncal VR, Hillier RJ, et al. Aqueous humor cytokines and long-term response to anti-vascular endothelial growth factor therapy in diabetic macular edema. *Am J Ophthalmol*. 2019;206:176−183.
26. Khorrami M, Khunger M, Zagouras A, et al. Combination of peri- and intratumoral radiomic features on baseline CT scans predicts response to chemotherapy in lung adenocarcinoma. *Radiol Artif Intell*. 2019;1(2):180012.
27. Braman N, Prasanna P, Whitney J, et al. Association of peritumoral radiomics with tumor biology and pathologic response to preoperative targeted therapy for HER2 (ERBB2)−positive breast cancer. *JAMA Netw Open*. 2019;2(4). e192561-e192561.
28. Beig N, Khorrami M, Alilou M, et al. Perinodular and intranodular radiomic features on lung CT images distinguish adenocarcinomas from granulomas. *Radiology*. 2018;290(3):783−792.
29. Henaine-Berra A, Garcia-Aguirre G, Quiroz-Mercado H, Martinez-Castellanos MA. Retinal fluorescein angiographic changes following intravitreal anti-VEGF therapy. *J AAPOS*. 2014;18(2):120−123.
30. Allingham MJ, Mukherjee D, Lally EB, et al. A quantitative approach to predict differential effects of anti-VEGF treatment on diffuse and focal leakage in patients with diabetic macular edema: a pilot study. *Transl Vis Sci Technol*. 2017;6(2):7.
31. Ehlers JP. Peripheral and macular retinal vascular perfusion and leakage in DME and RVO (PERMEATE). Available at: https://clinicaltrials.gov/ct2/show/NCT02503540. Accessed January 12, 2020.
32. Moosavi A, Figueiredo N, Prasanna P, et al. Imaging features of vessels and leakage patterns predict extended interval aflibercept dosing using ultra-widefield angiography in retinal vascular disease: findings from the PERMEATE Study. *IEEE Trans Biomed Eng*. 2021;68(6):1777−1786.